Received: 21 September 2018 | Revised: 8 December 2018 | Accepted: 10 December 2018

DOI: 10.1002/rcm.8371

RESEARCH ARTICLE

WILEY Rapid Communications in Mass Spectrometry

Investigations into the performance of travelling wave enabled conventional and cyclic ion mobility systems to characterise protomers of fluoroquinolone antibiotic residues

Michael McCullagh | Kevin Giles | Keith Richardson | Sara Stead | Martin Palmer

Waters Corporation, Stamford Avenue, Altrincham Road, Wilmslow SK9 4AX, UK

Correspondence
Michael McCullagh, Waters Corporation, Stamford Avenue, Altrincham Road, Wilmslow SK9 4AX, UK.
Email: mike_mccullagh@waters.com

Rationale: Fluoroquinolones (FLQs) have been shown to form protomers with distinctive fragment profiles. Experimental parameters affect protomer formation, impacting observed conventional tandem mass spectrometric (MS/MS) dissociation and multiple reaction monitoring (MRM) transition reproducibility. Collision cross section (CCS) measurement can provide an additional identification metric and improved ion mobility (IM) separation strategies could provide further understanding of fluctuations in fragmentation when using electrospray ionisation (ESI).

Methods: Porcine muscle tissue was fortified with nine fluoroquinolone antibiotics. Extracts were cleaned using QuEChERS dispersive extraction. Separation was achieved via ultra-high-performance liquid chromatography (UHPLC) and analysis performed using positive ion ESI coupled with linear T-wave IM (N_2 and CO_2 drift gas) and cyclic IM-MS (calibrated to perform accurate mass and CCS measurement).

Results: IM-resolved protomeric species have been observed for nine FLQs (uniquely three for danofloxacin). Long-term reproducibility and cross-platform T-wave/cIM studies have demonstrated CCS metric errors <1.5% when compared with a FLQ protomer reference CCS library. When comparing FLQ protomer separation using a standard, linear T-wave IM separator (N_2/CO_2) and using a high-resolution cyclic T-wave device (N_2), protomer peak-to-peak resolution ranged between Rs = 1 to Rs = 6 for the IM strategies utilised.

Conclusions: CCS is a reliable cross platform metric; specific FLQ CCS identification fingerprints have been produced, illustrating the potential to compliment MS/MS specificity or provide an alternative identification metric. Using cIM there is opportunity to correlate the erratic nature of protomer formation with the analytical conditions used and to gain further understanding of ionisation/dissociation mechanisms taking place during routine analyses.

1 | INTRODUCTION

Due to concerns regarding the spread of antibiotic-resistant microorganisms in the human population, the USA Food and Drug Administration introduced a ban on the use of enrofloxacin and ciprofloxacin fluoroquinolones (FLQs) in livestock production in 2005.[1,2] The use of antibiotic growth-promoting agents (AGPs) in animal husbandry has been forbidden in the European Union (EU) since 2006.[3] EU MRLs currently exist for eight FLQ compounds and are dependent on the species and tissue type.[4] The FLQs are chemically diverse zwitterionic species possessing a basic 4-quinolone ring structure; functional group modifications around the quinolone ring (benzopyridone nucleus) improve the antimicrobial potency.

The typical requirements for FLQ residue analysis are a solvent extraction step followed by solid-phase extraction (SPE) purification and detection using liquid chromatography/ultraviolet (LC-UV),

LC/mass spectrometry (MS) or fluorescence.[5] Many different types of mass analysers are routinely utilised for veterinary drug residue (VDR) analysis, including single quadrupole, ion trap and more recently time-of-flight (TOF)-based technologies.[6-8] However tandem quadrupole MS using multiple reaction monitoring (MRM) with its selectivity/sensitivity benefits has gained widespread acceptance.[9-12] The identification acceptance criteria for this approach are defined in the European Commission Decision 2002/657/EEC, which regulates the requirements for analytical methods used to quantify and confirm VDRs in food and animal feeds.[13] When choosing to implement a new tandem quadrupole based method for VDR analysis, the selection of the most appropriate MRM transitions is critical and must be performed and validated in accordance with the 2002/657/EC guidelines. Meeting the set criteria for acceptable precursor/product ion ratio tolerances can prove challenging due to erratic variations in the analytical responses obtained. An understanding of the impact of matrix on response reproducibility was provided by Kaufmann et al,[6] who reported protomer separation of FLQs for the first time using ion mobility (IM), with each protomer generating distinctive product ions. Relative protomer intensity was shown to be impacted by cone voltage, desolvation temperature and matrix, ultimately causing variance in observed product ion ratios. Subsequently, a number of other studies into protomer formation and analysis using IM have been undertaken.[14-18]

IM-based separation of compounds is dependent on ionic size, shape and charge differentiation. It provides an added dimension of separation to MS analysis, increasing peak capacity and providing a means to determine collision cross-section (CCS) values, an additional analyte identification metric. Using CCS values can increase targeted screening specificity. CCS searchable data bases have been created across multiple areas of research including natural product screening/metabolism, veterinary drugs, metabolomics, lipids, mycotoxins, steroids and steviosides.[18-27] IM separations of chromatographically coeluting isomers of metabolites, *C*6/*C*8 glycosidic flavonoids and isomer direct analysis have also been performed.[28-32]

The use of IM separation for small molecule analysis has increased across many application areas. An approach in which it is possible to identify FLQ protomers (gas-phase isomers differentiated only by their protonation site) using accurate mass measurement in conjunction with CCS measurement, without relying on characteristic fragmentation ratios, could be beneficial, for example, at low concentrations, where product ions may be weak or unobserved; IM separation could also provide a further confirmatory, differentiating metric for protomers (where fragmentation has been observed).

Ultra-high-performance liquid chromatography (UHPLC)/IM-TOFMS to detect multiple protonation sites and different fragmentation patterns within the FLQ class of antibiotics has been performed. It can be used as an important method development tool to support the unequivocal identification of FLQ antibiotics in crude tissue extracts. An in-house reference CCS library has been generated using FLQ standards enabling comparison with the measured values, to screen/confirm FLQ protomer formation, facilitating studies into the impact of assay conditions employed. We explore strategies to improve IM separation of the FLQ protomers, as a function of IM gas polarisability (N_2 and CO_2) and using an alternate, high IM resolution instrument design.[33]

2 | EXPERIMENTAL

2.1 | Materials and methods

2.1.1 | Preparation of samples and chemical materials

Extracts

Ground pork (10 g; 5% fat) was placed into a 50 mL centrifuge tube and 20 mL acetonitrile were added. The mixture was shaken vigorously for 1 min. The contents of DisQuE pouch salts for European Committee for Standardization (CEN method 15662) QuEChERS were added and shaken vigorously for 1 min then centrifuged for 3 min at 6000 rpm. 10 mL aliquots of the supernatant from three extracts were combined and chilled in two Falcon tubes at −18°C for 15 min. Then 10 mL of hexane were added to each tube and shaken for 30 s. After centrifuging for 5 min at 6000 rpm the hexane layer was discarded. The acetonitrile layer was filtered through a 0.2 μm nylon filter and one aliquot fortified with FLQs standards.

Analytes: FLQ standards

Standard solutions (100 ng/mL) of norfloxacin, ciprofloxacin, enoxacin, marbofloxacin, enrofloxacin, danofloxacin, sarafloxacin, difloxacin and lomefloxacin were prepared. Mobile phases comprised acetonitrile, H_2O and formic acid (all purchased from Sigma Aldrich, Poole UK).

2.1.2 | Chromatographic conditions

UHPLC analyses were performed using a Waters ACQUITY UPLC I-Class chromatograph and a Waters ACQUITY UPLC BEH C_{18} (100 mm × 2.1 mm, 1.7 μm) column at 40°C. The mobile phase consisted of solvent A (0.1% formic acid in H_2O) and solvent B (0.1% formic acid in acetonitrile). Reversed-phase separations (0.6 mL/min) were performed using a linear gradient elution programme: 0–1 min isocratic at 98:2 (A:B); 1–8 min, (70:30), 8–9 min (50:50), 9.5 min (5:95), 9.6–11.5 min (98:2).

2.1.3 | Ion mobility mass spectrometry conditions

Two IM-MS instruments were used in this study; a Synapt G2-*Si* instrument (Waters Corp., Wilmslow UK) and a research platform based on a Synapt G2-*Si* with the standard, linear, IM cell replaced by a multi-pass cyclic IM cell for increased mobility resolution. Both systems utilise Travelling Wave (TW) mobility separation which is described in more detail elsewhere.[34-36]

Synapt G2-*Si*

The Synapt G2-*Si* was coupled with the chromatographic system described above. The mass spectrometer was mass calibrated in positive ion electrospray mode at 20,000 resolution full width at half maximum (FWHM) determined at *m/z* 556. The reference lockmass calibrant was leucine enkephalin ($[M+H]^+$ at *m/z* 556.2766) at 200 pg/μL (water/acetonitrile (50:50, v/v) + 0.1% formic acid) infused at 10 μL/min. Using default ion mobility protocol parameters,

IM resolution was ≈ 40 Ω/ΔΩ (FWHM). Calibration of the IM cell for $CCSN_2$ calculations was performed using an IMS/TOF calibration kit (Waters Corp.). Bush et al[37] previously presented the T-wave ion mobility calibration strategies.

Default IM screening parameters include: TW Velocity Ramp = Start: 1000 m/s End: 300 m/s.[38] TW Pulse Amplitude = 40 V and gas flows of 180/90 mL/min for the respective helium/IM cells, giving an IM cell pressure of ~3.2 mbar. Capillary/cone voltages of 1 kV/30 V were applied. A nitrogen desolvation gas flow of 1000 L/h and desolvation temperature of 550°C were used. The source temperature was set at 150°C. The mass spectrometer was operated in the data-independent $HDMS^E$ acquisition mode whereby after the separated precursor ions exit the IM cell, they are fragmented in one scan function and transmitted intact in another. Consequently, both precursor and product ion information was obtained from a single injection. A default, collision energy of 4 eV was employed in the low-energy function and the high-energy function utilised a collision energy ramp (15 to 45 eV). Argon was used for collision-induced dissociation (CID). All data were acquired over the mass range of *m/z* 50–1200, at an acquisition rate of 10 spectra per second.

Cyclic ion mobility (cIM) research platform

The cIM device in a modified Synapt provides a longer mobility separation path length and, consequently, higher mobility resolution than the standard linear TWIM cell; in addition, the multi-pass capability can provide significantly higher resolution over a reduced (selected) mobility range. The cIM device consists of a 100 cm path length radiofrequency (RF) ion guide comprising over 600 electrodes around which TWs circulate to provide mobility separation.[33]

The cIM instrument was also coupled with the chromatographic system described above and direct infusion. The mass spectrometer was mass calibrated in positive ion electrospray mode at 60,000 resolution FWHM over an *m/z* range of 50–1000 using an IMS/TOF calibration kit (Waters Corp.). The reference lockmass calibrant was sodiated raffinose ($[M + Na]^+$ *m/z* 527.1583) at 1000 pg/μL (water/acetonitrile (50:50, v/v)) infused at 10 μL/min. IM resolution was ≈ 65 Ω/ΔΩ (FWHM) for a single pass around the cIM device; resolution increases with the square root of the number of passes.

IM parameters include: cIM T-wave velocity = 353 m/s, T-wave pulse amplitude = 25 V and gas flows of 120/25 mL/min for the respective helium/IM cells resulting in an IM pressure of 2.7 mbar. Capillary/cone voltages of 1 kV/30 V were applied. A nitrogen desolvation gas flow of 800 L/h and desolvation temperature of 550°C were used. The source temperature was set at 120°C. Data were acquired using HDMS or HDMSMS acquisitions; product ion data were acquired with fixed collision energies (15, 20, 30 and 40 eV) using nitrogen as the collision gas. All data were acquired at 2 spectra per second.

2.1.4 | Data processing

Data were acquired on the Synapt G2-*Si* using MassLynx 4.1 SCN 916/924. UNIFI 1.8 software (Waters Corp.) was used for data processing, alignment of the precursor/IM product ions and extraction of CCS values and %CCS error from the data. Initially apex peak detection/centroiding of the data is performed, where candidates are created and compared to the library database.[39] The post-peak detection processing parameters applied have previously been described for CCS pesticide screening.[15] For Synapt data the reference CCS library values for the FLQ protomer values were generated in-house.

The cIM-based instrument control and data acquisition were facilitated by in-house software comprising a novel web-based user interface and a modified version of Masslynx 4.1. CCS values were determined for single pass separation by using DriftScope 2.9 (Waters Corp.) and manual calibration using Waters' standard calibration form.

3 | RESULTS AND DISCUSSION

3.1 | Characterisation of fluoroquinilone protomers and generation of CCS fingerprints

IM-MS on the Synapt G2-S*i* was used as tool to support the unequivocal identification of FLQ antibiotic residues in crude porcine tissue extracts. Characterisation of protomeric species from nine FLQs (see Figure 1) produced from standards using a routine CCS screening workflow has been performed. Estimated $^{TW}CCSN_2$ values of the protomers formed for each FLQ have been determined in-house and incorporated into a reference library (generated in 2015 and not previously published).

Building on the work of Kaufman et al,[6] extensive investigation and elucidation of the fragmentation mechanisms of FLQs was carried out.[14-18] Wang et al[14] illustrated that the MS/MS fragmentation patterns of four drug-like compounds were not only affected by the pH, but also by the aqueous-organic ratio of the mobile phase and the buffer concentration at a given pH. Neta et al[15] showed the impact of collision energy/cone voltage on protomeric species formation from quinolone drugs and extensively elucidated dissociation mechanisms (using density functional theory (DFT)), for producing H_2O and CO_2 neutral losses. Protomeric species intensity was shown to be impacted by dehydration/rehydration reactions. It was concluded that MRM transitions for certain complex compounds may be comparable only when monitored under equivalent ion-forming conditions.

Lapthorn et al[16] and Kovačević et al[17] have explored the potential of combined IM-MSMS with molecular modelling (DFT), for increased understanding of "small-molecule" dissociation pathways. There was agreement that for a 4-quinolone, the keto-oxygen (equivalent to O-17 in danofloxacin, Figure 1) is the most favoured site for protonation, exhibiting higher proton affinity than the N-19 and N-22 of the piperazine ring, which exhibit similar proton affinities. It may therefore be expected that a protomeric species characterised by the charge-mediated loss of H_2O would be observed. Opinions differed with respect to assignment of protonation on the carboxyl oxygen (equivalent to O-15, Figure 1), to form a third protomeric species (Lapthorn et al[16]). Kovačević et al[17] fully described the calculated proton affinities for the above-mentioned sites of protonation in both the gas and aqueous phases (where stability order is reversed and the most stable protomeric species would form

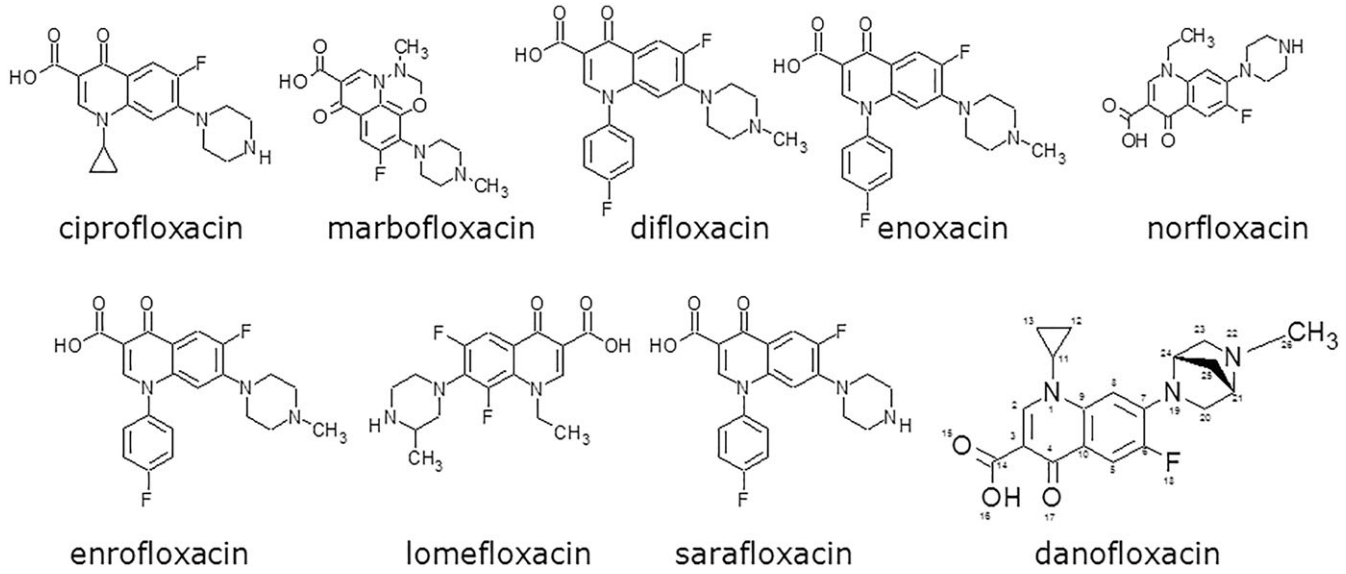

FIGURE 1 FLQs for which IM separation of protomers was performed

at the N-22 position). Proton affinity calculations clearly demonstrated that the basicities of piperazinyl quinolones undergo a reversal when entering the gas phase from solution. The potential formation/dissociation mechanisms of the protomeric species have been discussed extensively, together with studies of the fate of the observed $[M + 2H]^{2+}$ ions.

Relative protonation at differing sites within the same molecule in gas-phase ESI experiments can depend on source geometry, capillary voltage, solvent composition (gradient), pH, droplet size, desolvation temperature, flow rate and matrix. The resultant protomeric species ratios can affect the composite CID spectrum which, in turn, may impact the ratio of the intensities of recorded MRM traces produced when using tandem quadrupole MS. This is problematic since identification is confirmed if the ratios recorded are equal to those obtained for the analyte in pure standard, along with equivalent chromatographic retention times.

The UPLC BPI (base peak intensity) chromatogram of the nine FLQs, obtained on the Synapt G2-*Si*, is shown in Figure 2. The corresponding plot of ion mobility arrival time (N_2 IM gas) vs retention time (upper plot in Figure 2) reveals 18 identified FLQ ion species. For each individual FLQ chromatographic peak, the corresponding ion mobility peak detection resulting from two separated species is shown (produced by different sites of protonation for each of the listed molecules). Measured $^{TW}CCSN_2$ differences of 10–15 Å^2 were observed for the protomeric pairs. When compared with the $^{TW}CCSN_2$ 2015 in-house reference library, differences of <1.1% were obtained (see Table 1). The observed FLQ protomer CCS values result from differences in long-range interactions between the different protonated species and the IM drift gas.

Lapthorn et al[40] investigated IMS using the drift gases with decreasing polarisability (CO_2 > N_2 > He), to separate FLQ protomers. Using a RF confining linear field drift cell they showed that FLQ

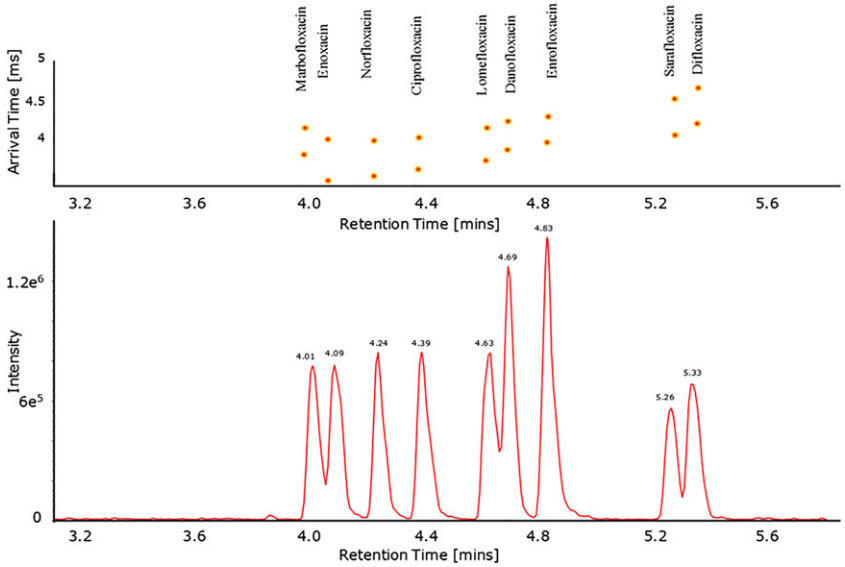

FIGURE 2 Expanded BPI chromatogram for a mixture of nine FLQs (lower plot) and component arrival time plot (upper), for peak detection of nine pairs of FLQ protomers corresponding to each chromatographic peak [Color figure can be viewed at wileyonlinelibrary.com]

TABLE 1 Reference FLQ protomer $^{TW}CCSN_2$ values (Synapt 2015) with observed $^{TW}CCSN_2$ (Synapt 2018, this study) and $^{TW}CCSN_2$ (cIM 2018, this study). Additionally, FLQ protomeric peak-to-peak resolution using the Synapt (N_2/CO_2 drift gas) and N_2 drift gas (1 and 3 passes) for the multi-pass cIM instrument

Protomer species	Observed *m/z*	Mass error (ppm)	Rt (min)	Reference $^{TW}CCSN_2$ Å^2 2015 Synapt	Observed $^{TW}CCSN_2$Å^2 2018 Synapt	$^{TW}CCSN_2$ error (%)	Observed $^{TW}CCSN_2$ Å^2 2018 cIM 1 pass	$^{TW}CCSN_2$ Å^2 error (%)	$^{TW}Rs^{P\text{-}P}$ N_2 Synapt	$^{TW}Rs^{P\text{-}P}$ CO_2 Synapt	$^{TW}Rs^{P\text{-}P}$ N_2 cIM 1 pass	$^{TW}Rs^{P\text{-}P}N_2$ cIM 3 pass	Adduct
Marbofloxacin I	363.1466	0.76	4	178.7	178.6	−0.07	178.1	0.35					+H
Marbofloxacin II	363.1466	0.76	4	189.9	189.0	−0.44	189.3	0.30	1.25	2.82	1.21	2.85	+H
Enoxacin I	321.1359	0.33	4.1	169.2	169.1	−0.01	169.6	−0.27					+H
Enoxacin II	321.1358	0.31	4.1	187.4	185.4	−1.04	186	0.74	1.97	3.08	2.68	5.66	+H
Norfloxacin I	320.1400	−1.41	4.25	171.6	170.9	−0.38	171.9	−0.20					+H
Norfloxacin II	320.1401	−1.39	4.25	185.7	185.0	−0.42	185.3	0.24	1.35	4.13	1.86	4.55	+H
Ciprofloxacin I	332.1402	−0.79	4.4	174.2	173.4	−0.49	174.2	0.02					+H
Ciprofloxacin II	332.1402	−0.79	4.4	187.1	185.0	−0.66	186.5	0.32	1.02	2.96	1.61	3.81	+H
Lomefloxacin I	352.1475	2.22	4.63	176.8	176.4	−0.22	174.2	1.52					+H
Lomefloxacin II	352.1475	2.22	4.63	191.3	189.3	−1.05	189.8	0.77	1.77	3.05	1.45	3.65	+H
Danofloxacin I	358.1555	−1.68	4.7	181.7	180.5	−0.62	183.7	−1.11					+H
Danofloxacin II	358.1555	−1.68	4.7	193.7	191.7	−1.04	194	−0.14	1.08	2.99	1.26	3.16	+H
Enrofloxacin I	360.1717	−0.29	4.84	184.2	183.5	−0.41	183.6	0.33					+H
Enrofloxacin II	360.1717	−0.27	4.84	194.7	193.5	−0.63	194	0.37	0.97	2.77	1.18	2.71	+H
Sarafloxacin I	386.1310	−0.24	5.26	187.2	185.8	−0.75	186.3	0.49					+H
Sarafloxacin II	386.1310	−0.24	5.26	201.2	200	−0.61	199.6	0.79	1.43	2.61	1.70	3.28	+H
Difloxacin I	400.1467	−0.04	5.35	192.1	190.1	−1.04	190.4	0.9					+H
Difloxacin II	400.1467	−0.05	5.35	205.1	204	−0.56	203.3	−1.1	1.40	2.87	1.59	3.80	+H

protomer IM peak separation was lost using He as a drift gas and retained using N_2. These observations indicate that the observed FLQs protomer separations are due to ionic charge distribution and its interaction with the drift gas, where the higher polarisability of N_2 leads to stronger long-range interactions. Theoretical CCS calculations were also performed demonstrating that significant differences in CCS can result from changes in charge distribution, not just physical size.

The danofloxacin $[M + H]^+$ *m/z* 358.15 protomers have IM arrival times of 3.84 ms (I) and 4.20 ms (II), with measured $^{TW}CCSN_2$ values of 180.6Å^2 and 191.6Å^2, respectively (see Figure 3). Post-mobility fragmentation spectra of the danofloxacin protomers, I and II, are shown in Figure 4. Based on previous studies,[14-18] protomer I has the proton on the keto group (O-17) and protomer II has the proton on the either the N-22 or N-19 (slightly less favourable) of the piperazine ring. Fragmentation of protomer I is via conformational change; the COOH group rotates producing a less stable conformer resulting in the neutral loss of H_2O giving rise to the product ion at *m/z* 340.15. Fragmentation of protomer II results from the remote charge-directed neutral loss of CO_2, creating the observed product ion at *m/z* 314.16. H_2O cannot be eliminated from protomer II because there is no acidic proton available adjacent to the carboxylic acid group. The characteristic FLQ protomer product ions determined (<5 ppm error) are summarised in Table S1 (supporting information).

As reported by Kaufmann et al,[6] the presence of more than one protonation site for the FLQs is confirmed by the observation of the $[M + 2H]^{2+}$ doubly charged species in the mass spectra. In addition to fragmentation information this evidence further suggests two sites of protonation, taking place on the acyl group and the piperazine ring. Through extension of the IM calibration protocol, the $^{TW}CCSN_2$ measurements of the doubly charged species have been made here, creating a $^{TW}CCSN_2$ fingerprint for each FLQ (see Table S2, supporting information). The combined IMS arrival time plot for the danofloxacin (protomers I and II) singly charged species $[M + H]^+$ *m/z* 358.15 and $[M + 2H]^{2+}$ doubly charged species, with the inset doubly charged danofloxacin spectrum *m/z* 179, is shown in Figure S1 (supporting information). For each of the singly charged protomer pairs, $Rs^{p\text{-}p}$ (peak-to-peak resolution) values between 0.97 and 1.97 were determined using N_2 as the IM gas (see Table 1) and therefore can be considered to be resolved.

3.2 | Enhancement in peak-to-peak resolution of fluoroquinolone protomers and identification of additional fluoroquinolone protomeric species

Interestingly, Lapthorn et al[16] reported three ion mobility species for norfloxacin (and an atypical mobility peak shape for one of the components indicating a potential fourth). It was proposed that the third, low intensity and shortest arrival time, isomer originated from the carbonyl oxygen (O-15 equivalent position in danofloxacin, Figure 1). This third protomeric species identified was described as being similar to a mixture of the two primary protomeric species, in that the presence of an ion at *m/z* 302 in the mass spectrum indicated a loss of H_2O from the precursor at *m/z* 320 (similar to protomer I) and the presence of *m/z* 276/*m/z* 256 indicated a loss of CO_2/HF (similar to protomer II). In this study, the FLQ data from the linear TWIM (Synapt G2-*Si*) system were interrogated further. In each case the extracted ATDs corresponding to a loss of CO_2 from the FLQ precursor were generated to establish the presence of additional protomer species (following Lapthorn et al). Using this methodology, additional peaks were identified in the extracted ATDs, with arrival times slightly shorter than those of the corresponding protomer I (see Table S3, supporting information).

To further investigate the potential formation of more than two protomeric forms of the FLQs, two approaches were used here to improve the IM separation capability. The first was to change the IM gas from N_2 to CO_2 on the Synapt G2-*Si*, the increased polarisability of CO_2 (CO_2 2.91×10^{-24} cm^3 vs N_2 1.74×10^{-24} cm^3) having been shown previously to improve separation.[41-44] The second approach was to use the novel multi-pass cIM instrument to provide increased mobility resolution through longer path-length separation.

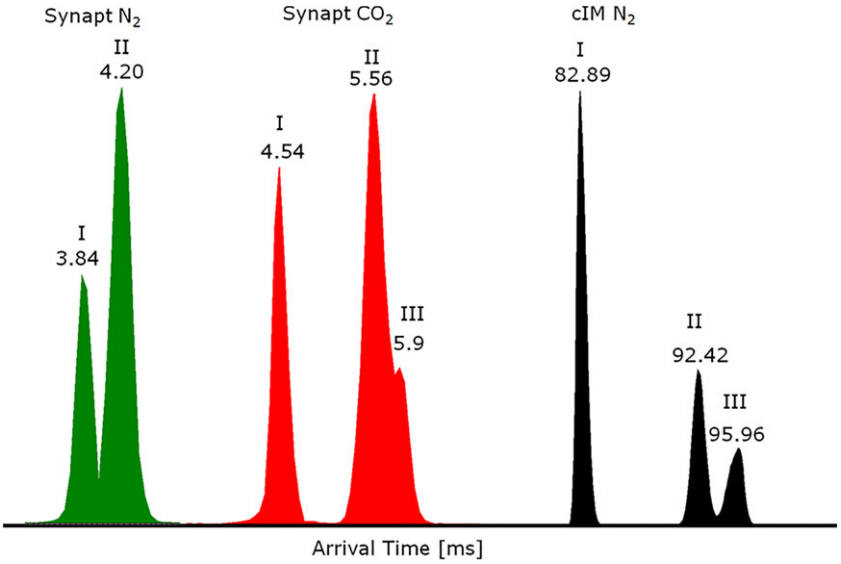

FIGURE 3 Danofloxacin IM protomer separation using the Synapt (N_2 and CO_2 IM gas) and cIM (N_2 IM gas, 5 passes) systems [Color figure can be viewed at wileyonlinelibrary.com]

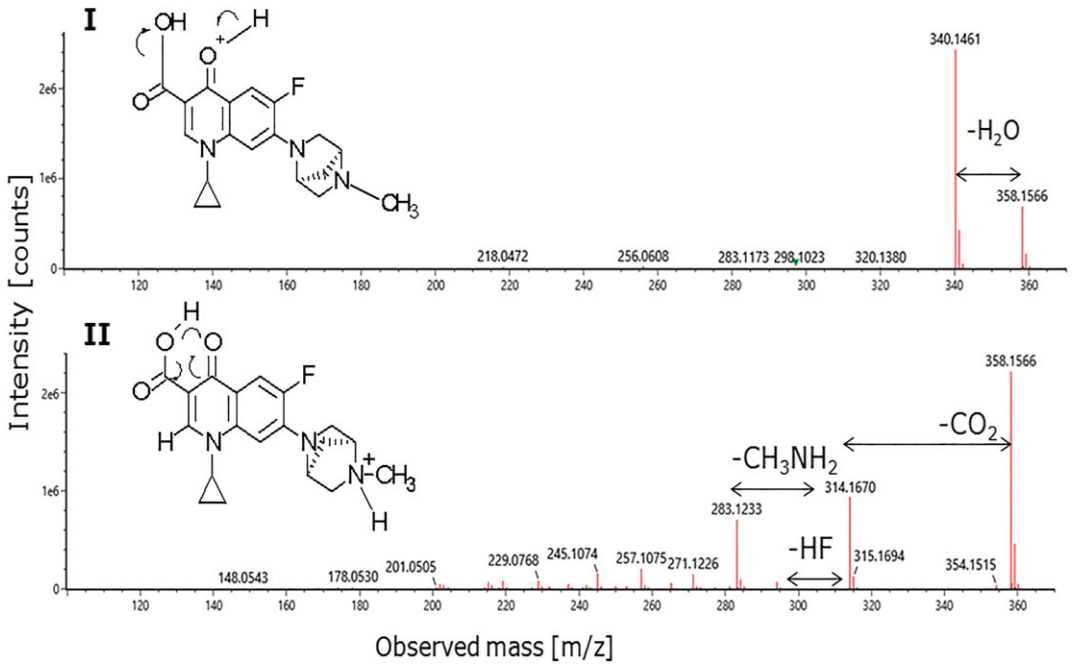

FIGURE 4 Product ion mass spectra of IM-separated (Synapt) danofloxacin protomers I and II [Color figure can be viewed at wileyonlinelibrary.com]

Using CO_2 as the drift gas, improved separation was seen for all protomer pairs, with $Rs^{P\text{-}P}$ ranging from 2.61 to 4.13 for the nine FLQs (see Table 1). No direct evidence of a third protomer was obvious from the extracted precursor ATDs, with the exception of danofloxacin where evidence of a third protomer was apparent: ATD I (4.54 ms) and overlapping ATDs II/III (at arrival times 5.56 and 5.90 ms), as shown in Figure 3. When post-mobility fragmentation is employed, ATD I is characterised by H_2O loss and ATDs II/III are characterised by the loss of CO_2. This observation will be discussed below.

The UPLC separation of the nine FLQs followed by one-pass cIM analysis (resolution ~65 Ω/ΔΩ) provided CCS values in good agreement with the library values (see Table 1) and $Rs^{P\text{-}P}$ values in the range of 1.18 to 2.68 which are similar to, or larger than, the N_2 values obtained on the Synapt G2-*Si*. Undertaking three passes around the cIM (resolution ~110 Ω/ΔΩ), $Rs^{P\text{-}P}$ values between 3.05 and 6.01 (see Table 1) were obtained, which are notably better than the equivalent CO_2 values from the linear TWIM separation. The enhanced separation of the $[M+H]^+$ ATDs observed for the cIM separation of norfloxacin, ciprofloxacin and enoxacin is shown in Figure 5. Under these conditions, in agreement with the CO_2 data, only danofloxacin showed clear evidence of a third protomer $[M+H]^+$ mobility peak and, at five passes around the cIM (resolution ~145 Ω/ΔΩ), the three protomeric species of danofloxacin were fully resolved, as can be seen in Figure 3. For protomers I/II, values of $Rs^{P\text{-}P} = 2.49$, for protomers II/III, $Rs^{P\text{-}P} = 2.2$, and, for protomers I/III, $Rs^{P\text{-}P} = 4.64$ were obtained. It is interesting to note that the skeletal structures of danofloxacin, difloxacin, ciprofloxacin are similar but that only danofloxacin exhibits three protomeric species. It is notable that the piperazine ring of danofloxacin is bridged between C25, C24 and C21. Interpretation of the observed danofloxacin data, might be

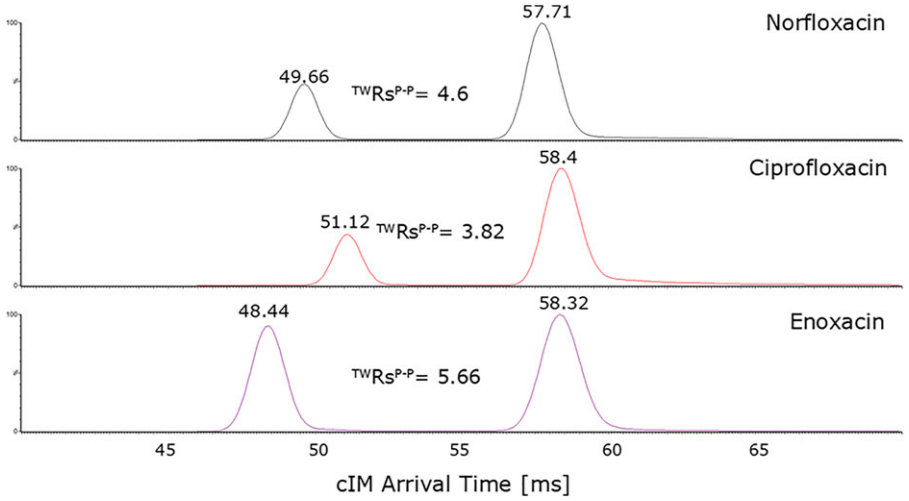

FIGURE 5 cIM separation of FLQ $[M+H]^+$ protomer pairs: cIM resolution (110 Ω/ΔΩ) [Color figure can be viewed at wileyonlinelibrary.com]

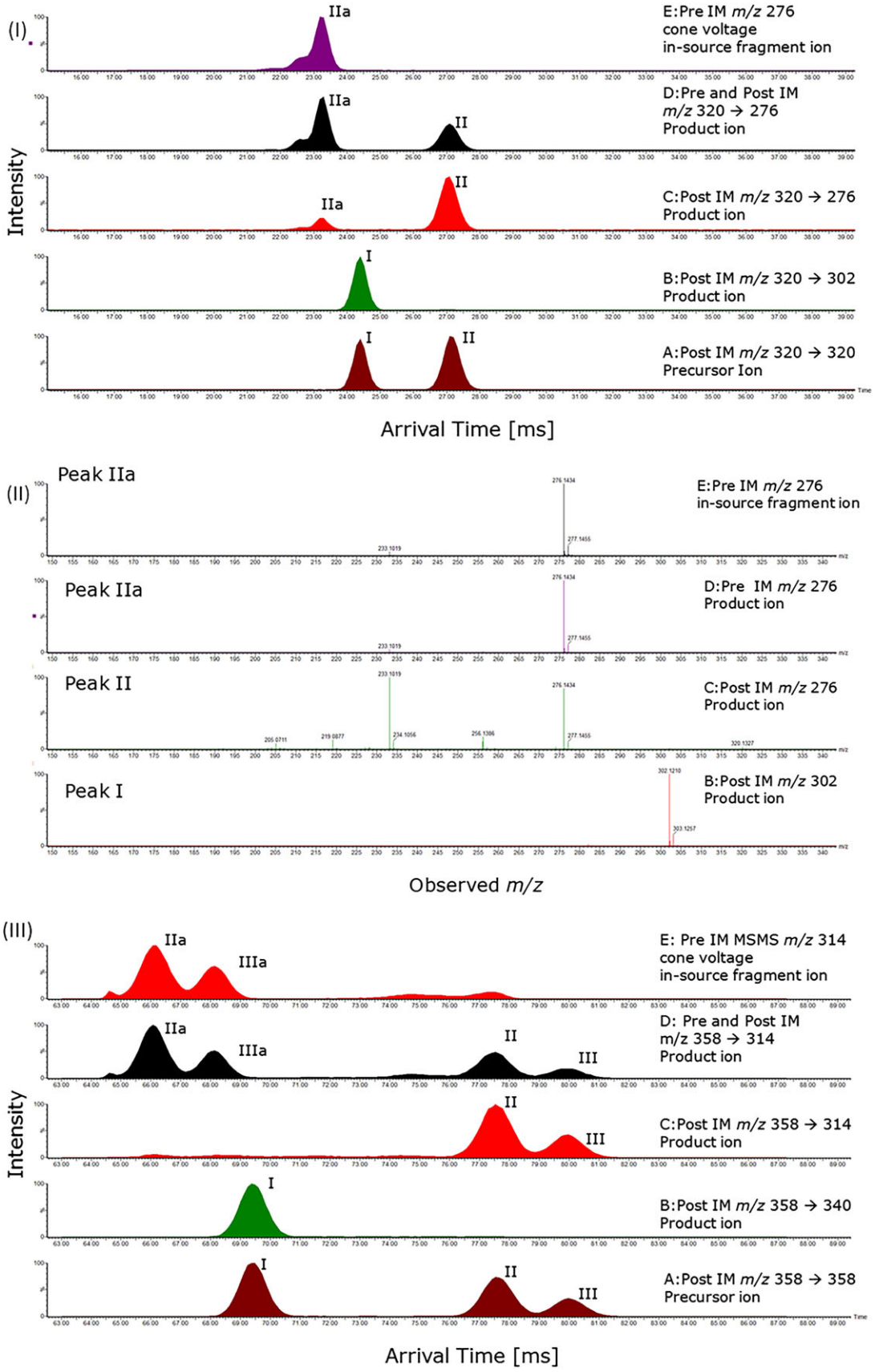

FIGURE 6 (I) cIM separation of norfloxacin FLQ protomers and pre-IM FLQ fragment ions for the MSMS transitions labelled (3 passes/resolution ~110 Ω/ΔΩ). (II) Dissociation spectra of cIM-resolved norfloxacin FLQ protomers and pre-IM FLQ fragment ions. (III) cIM-resolved danofloxacin FLQ protomers and pre-IM fragment protomer ions (4 passes/resolution ~130 Ω/ΔΩ)) for the MSMS transitions labelled [Color figure can be viewed at wileyonlinelibrary.com]

assisted by conformational analysis of each protomer, where all structures are optimized using DFT calculations, to generate the corresponding theoretical CCS values.[45]

Whilst it has not been demonstrated here, Giles et al have shown that increasing the number of passes on the cIM results in a maximum signal drop of 15% from 1 to 6 passes.[46]

Since no significant evidence for additional protomers from the $[M+H]^+$ species (with the exception of danofloxacin) had been apparent from the higher separation capability of the CO_2 and cIM, further studies were performed for norfloxacin (using MSMS selectivity) to try and understand the observed peaks in the CO_2 loss fragment ion spectra observed by Lapthorn et al and the present Synapt data. Using the selectivity of MSMS the FLQ norfloxacin *m/z* 320 was selected using the quadrupole and additional IM investigations performed. Figure 6(I(A)) shows the ATD for cIM (3 passes, resolution ~110 Ω/ΔΩ) resolved $[M+H]^+$ *m/z* 320 precursor ion (*m/z* selected using the quadrupole) for norfloxacin (ATD A:*m/z* 320), where only two protomers are apparent. In Figures 6(I(B,C)) the post-IM protomer fragment ion ATDs resulting from the loss of H_2O/CO_2 are shown (H_2O loss (ATD B: *m/z* 302) and CO_2 loss (ATD C: *m/z* 276)). Interestingly, in the CO_2 loss ATD, an additional peak (IIa) is apparent which is fully resolved from ATD (I). Peak IIa confirms the additional peak observed by Lapthorn et al and the present linear TWIM data. However, with the higher resolution of the cIM it can be seen that there is no evidence of an $[M+H]^+$ protomer precursor (Figure 6(I(A))). In Figure 6(I(D)) additional pre-IM collision energy is applied which reveals that species D:ATD (IIa), *m/z* 276, increases in intensity and ATD (I), corresponding to a loss of CO_2 from norfloxacin, decreases in intensity, indicating that protomer species II/IIa are integrally linked. Finally, increasing the cone voltage to induce in-source fragmentation and selecting the *m/z* 276 fragment ion using the quadrupole generated the ATD shown in Figure 6(I(E)) where it can be seen that the arrival time matched that of ATD (IIa). It was therefore concluded that previously reported "mixed" ATD (I) spectra observed for norfloxacin resulted from some pre-IM fragmentation generating the CO_2 loss fragment which was then mobility separated. The corresponding mass spectra are shown in Figure 6(II). Interestingly, a shoulder can be seen on the leading edge of the *m/z* 276 IIa mobility peak in Figures 6(I(D,E)). The *m/z* 276 ATD has been investigated further (see Figure S3, supporting information). It can be seen that the shoulder can be increased by increasing cone voltage (Figure S3(I,II)) and that at higher mobility resolution the shoulder splits into two peaks. Underlying interferences cannot be ruled out for this observation; however, there was no evidence of isobaric *m/z* 276 peaks and the post-IM fragmentation data performed on the ATDs (see Figure S3(III), supporting information) were similar with somewhat different intensity profiles. These observations will be investigated as part of a further study.

The enhanced separation of multi-protomeric species provided by the cIM device is informative and has provided an explanation of the mixed protomer dissociation spectra observed herein and by Lapthorn et al.[16]

Danofloxacin is an interesting case with the observation of three protomers and so has been investigated further. The $[M+H]^+$ *m/z* 358 protomer precursor ions (quadrupole selected) were separated using the cIM and then subjected to post-IM fragmentation and the corresponding, time-aligned, product ions for each protomer determined (see Figure S2, supporting information). It is observed that protomer I dissociation involves a primary loss of H_2O whereas protomers II and III have the same dissociation profile, but different intensities, with a primary loss of CO_2 (the time-aligned CO_2/H_2O product ion peaks are seen in in Figures 6(III(A,B,C)). It is possible that the similar product ion spectra observed for protomers II and III result from protonation at the N-19 and N-22 sites of the piperazine ring (shown for danofloxacin in Figure 1).

It was interesting to observe that two species were formed from partial pre-IM fragmentation generating the CO_2 loss fragment and were mobility separated, retaining the 'protomeric' form of the precursors. Figure 6(III) shows the *m/z* selected danofloxacin protomer precursor ATDs (I, II, III) *m/z* 358 (plot A) and the resultant characteristic FLQ dissociation product ions ATD (I) *m/z* 340 (plot B) and ATD (II/III) *m/z* 314 (plot C). Increasing the pre-IM trap collision energy (plot D) and pre-IM in-source fragmentation elevated the intensity of ATDs (IIa/IIIa) (plot E). These data reveal, for the first time, a combination of five protomeric species being generated for danofloxacin (resulting from two *m/z* 314 protomeric fragments and three *m/z* 358 precursor ion protomers). The origin of the ATD features between 73 and 78 ms in Figure 6(III(E)) are not clear and will be investigated in a further study. The danofloxacin post-IM fragmentation mass spectra are shown in Figure S2 (supporting information).

Overall, for the norfloxacin and the danofloxacin, the capability to increase the resolution of the cIM by increasing the number of passes has enabled separation of formerly unresolved components and, as such, improved understanding of previously observed FLQ 'mixed protomer' fragmentation data.

4 | CONCLUSIONS

Investigations into strategies to improve ion mobility separation of FLQ protomers, development of multi-protomeric $^{TW}CCSN_2$ fingerprints, have enabled construction of a FLQ $^{TW}CCSN_2$ reference library incorporating singly and doubly charged species. The FLQ reference library generated can be utilised to add specificity in a non-targeted screening approach, where, at low concentrations, product ions may be weak or unobserved. In the case of the FLQs, additional identification metrics (CCS values and distinctive dissociation patterns) have been generated to be utilised alongside retention time and accurate mass measurement. Strategies to enhance IM separation of FLQ protomer species, through choice of IM gas and novel instrumentation, increased measured $Rs^{P\text{-}P}$ values over that of the standard linear TWIM system (Synapt G2-*Si*, N_2 IM gas). In the case of danofloxacin a third protomer was partially resolved using linear TWIM with CO_2 IM and fully resolved with the cIM (N_2 drift gas) device. The enhanced cIM separation facilitated an understanding of previously observed 'mixed protomer' dissociation spectra, where single component fragmentation spectra were obtained.

There is opportunity with single component arrival time distributions to gain further understanding of ionisation/dissociation mechanisms taking place during routine analyses. It is possible that the specificity of UHPLC/IM-TOFMS can be used to provide

visibility of the impact of experimental parameters on protomer formation when developing MRM transition methods on tandem quadrupole instruments.

IM separation of protomers for other classes of compound has been identified, including, porphyrins, pesticides and pharmaceuticals.[19,45,47,48] An alternate strategy could be developed using multi-protomer CCS measurements as additional identification points. $^{TW}CCSN_2$ values have been determined here in combination with accurate mass measurement, retention time and characteristic ion mobility product ion spectra, providing a multi-metric fingerprint upon which alternate identification criteria could be based. The data presented illustrates long-term and cross platform $^{TW}CCSN_2$ reproducibility. Future investigations will utilise increased ion mobility separation to further understand the observations that have been made here and to further extend the reference $^{TW}CCSN_2$ database. A glossary of terms is available in the supporting information.

ORCID

Michael McCullagh https://orcid.org/0000-0003-4785-1745

REFERENCES

1. Final decision of the commissioner. Docket # 2000N-I 57 1, Withdrawal of the approval of the new animal drug application for enrofloxacin in poultry, Department of Health and Human Services, U.S. Food and Drug Administration
2. FDA Center for Veterinary Medicine. FDA Order Prohibits Extralabel Use of Fluoroquinolones and Glycopeptides. http://www.fda.gov/AnimalVeterinary/NewsEvents/CVMUpdates/ucm127904.htm. June 2, 1997.
3. Official journal of the European Union. L268:29–43, Regulation (EC) No 1831/2003 of the European Parliament and of the Council of 22 September 2003 on additives for use in Animal Nutrition
4. Official journal of the European Union. L24:1–8 Annex I, Council Regulation (EEC) No 2377/90 of 26 June 1990 laying down a Community procedure for the establishment of maximum residue limits of veterinary medicinal products in foodstuffs of Animal origin
5. Verdon E, Couedor P, Roudaut B, Sandérs P. Multiresidue method for simultaneous determination of ten quinolone antibacterial residues in multimatrix/multispecies animal tissues by liquid chromatography with fluorescence detection: Single laboratory validation study. *J AOAC Int*. 2005;88:1179-1192.
6. Kaufmann A, Butcher P, Maden K, Widmer M, Giles K, Uria D. Are liquid chromatography/electrospray tandem quadrupole fragmentation ratios unequivocal confirmation criteria? *Rapid Commun Mass Spectrom*. 2009;23(7):985-998.
7. Mol H, Zomer P, de Koning M. Qualitative aspects and validation of a screening method for pesticides in vegetables and fruits based on liquid chromatography coupled to full scan high resolution (Orbitrap) mass spectrometry. *Anal Bioanal Chem*. 2012;403(10):2891-2908.
8. Croley TR, White KD, Callahan JH, Musser SM. The chromatographic role in high resolution mass spectrometry for non-targeted analysis. *J Am Soc Mass Spectrom*. 2012;23(9):1569-1578.
9. Lucchetti D, Fabrizi L, Guandalini E, et al. Long depletion time of enrofloxacin in rainbow trout (*Oncorhynchus mykiss*). *Antimicrob Agents Chemother*. 2004;48(10):3912-3917.
10. Gajda A, Posyniak A, Zmudzki J, Gbylik M, Bladek T. Determination of (fluoro) quinolones in eggs by liquid chromatography with fluorescence detection and confirmation by liquid chromatography-tandem mass spectrometry. *Food Chem*. 2012;15:430-439.
11. McMullen SE, Schenck FJ, Vega VA. Rapid method for the determination and confirmation of fluoroquinolone residues in catfish using liquid chromatography/fluorescence detection and liquid chromatography tandem mass spectrometry. *J AOAC Int*. 2009;92:12312-12340.
12. Toussaint B, Chedin M, Bordin G, Rodriguez AR. Determination of (fluoro) quinolone antibiotic residues in pig kidney using liquid chromatography-tandem mass spectrometry. *J Chromatogr A*. 2005;1088(1-2):32-39.
13. Commission decision (2002/657EEC). Official Journal of the European Communities. 2002.
14. Wang J, Aubry A, Bolgar MS, et al. Effect of mobile phase pH, aqueous-organic ratio, and buffer concentration on electrospray ionization tandem mass spectrometric fragmentation patterns: Implications in liquid chromatography/tandem mass spectrometric bioanalysis. *Rapid Commun Mass Spectrom*. 2010;24(22):3221-3229.
15. Pedatsur N, Godugu B, Liang Y, Simón-Manso Y, Yang X, Stein SE. Electrospray tandem quadrupole fragmentation of quinolone drugs and related ions on the reversibility of water loss from protonated molecules. *Rapid Commun Mass Spectrom*. 2010;24(22):3271-3278.
16. Lapthorn C, Dines TJ, Chowdhry BZ, Perkins GI, Pullen FS. Can ion mobility mass spectrometry and density functional theory help elucidate protonation sites in 'small' molecules? *Rapid Commun Mass Spectrom*. 2013;27(21):2399-2410.
17. Kovačević B, Schorr P, Qi Y, Volmer DA. Decay mechanisms of protonated 4-quinolone antibiotics after electrospray ionization and ion activation. *J Am Soc Mass Spectrom*. 2014;25(11):1974-1986.
18. Chalet C, Hollebrands B, Janssen H, Augustijns P, Duchateau G. Identification of phase-II metabolites of flavonoids by liquid chromatography–ion-mobility spectrometry–mass spectrometry. *Anal Bioanal Chem*. 2018;410(2):471-482.
19. Pulkrabova J, Tomaniova M. 6th international symposium on recent advances in food analysis (RAFA), Prague, Czech Republic. November 5–8 2013.
20. Paglia G, Williams JP, Menikarachchi L, et al. Ion mobility derived collision cross sections to support metabolomics applications. *Anal Chem*. 2014;86(8):3985-3993.
21. Paglia G, Angel P, Williams JP, et al. Ion mobility-derived collision cross section as an additional measure for lipid fingerprinting and identification. *Anal Chem*. 2015;87(2):1137-1144.
22. Righettia L, Fenclovaa M, Dellafiorab L, Hajslovaa J, Stranska-Zachariasovaa M, Dall'Astab C. High resolution-ion mobility mass spectrometry as an additional powerful tool for structural characterization of mycotoxin metabolites. *Food Chem*. 2018;245:768-774.
23. Righetti L, Bergmann A, Galaverna G, Rolfsson O, Paglia G, Dall'Asta C. Ion mobility-derived collision cross section database: Application to mycotoxin analysis. *Anal Chim Acta*. Jul 19; 2018;1014:50-57.
24. Lipok C, Hippler J, Schmitz OJ. A four dimensional separation method based on continuous heart-cutting gas chromatography with ion mobility and high resolution mass spectrometry. *J Chromatogr a*. 2018;1536:50-57.
25. McCullagh M, Douce D, Van Hoeck E, Goscinny S. Exploring the complexity of steviol glycosides analysis using ion mobility mass spectrometry. *Anal Chem*. 2018;90(7):4585-4595.
26. Bauer A, Kuballa J, Rohn S, Jantzen E, Luetjohann J. Evaluation and validation of an ion mobility quadrupole time-of-flight mass spectrometry pesticide screening approach. *J Sep Sci*. 2018;41(10):2178-2187.
27. Hernández-Mesa M, Le Bizec B, Monteau F, García-Campaña AM, Dervilly-Pinel G. Collision cross section (CCS) database: An additional measure to characterize steroids. *Anal Chem*. 2018;90(7):4616-4625.
28. Gallagher R, Pattison C, Pickup K, Chipperfield J, McCullagh M, Douce D. Enhanced characterisation of metabolites using microflow UPLC-MS and collision cross section measurements. *Proceedings of the 62nd ASMS Conference on Mass Spectrometry and Allied Topics*, Baltimore, MD. June, 2014.

29. McCullagh M, Neeson K. Appl. Note Utilizing the increased peak capacity of UPLC ion mobility Tof MS and MS^E to overcome sample complexity. *Library number 720004336en*. Waters Corporation. 2012.
30. Fasciotti M, Sanvido GB, Santos VG, et al. Separation of isomeric disaccharides by traveling wave ion mobility mass spectrometry using CO_2 as drift gas. *J Mass Spectrom*. 2012;47(12):1643-1647.
31. Bataglion GA, Souza GH, Heerdt G, et al. Separation of glycosidic catiomers by TWIM-MS using CO_2 as a drift gas. *J Mass Spectrom*. 2015;50(2):336-343.
32. Ahonen L, Fasciotti M, Gennäsa GB, et al. Separation of steroid isomers by ion mobility mass spectrometry. *J Chromatogr a*. 2013;1310:133-137.
33. Giles K, Ujma J, Wildgoose J, et al. Design and performance of a second generation cyclic ion mobility enabled Q-TOF. *Proceedings of the 65th ASMS Conference on Mass Spectrometry and Allied Topics*, Indianapolis, 2017. TP385
34. Giles K, Pringle SD, Worthington KR, Little D, Wildgoose J, Bateman RH. Applications of a travelling wave-based radio-frequency only stacked ring ion guide. *Rapid Commun Mass Spectrom*. 2004;18:2401.
35. Pringle SD, Giles K, Wildgoose J, et al. An investigation of the mobility separation of some peptide and protein ions using a new hybrid quadrupole/travelling wave IMS/oa-ToF instrument. *Int J Mass Spectrom*. 2007;261(1):1-12.
36. Lalli PM, Iglesias BA, Toma HE, et al. Protomers: Formation, separation and characterization via travelling wave ion mobility mass spectrometry. *J Mass Spectrom*. 2012 Jun;47(6):712-719.
37. Bush MF, Campuzano I, Robinson CV. Ion mobility mass spectrometry of peptide ions: Effects of drift gas and calibration strategies. *Anal Chem*. 2012;84(16):7124-7130.
38. Eckers C, Laures AMF, Giles K, Major H, Pringle S. Evaluating the utility of ion mobility separation in combination with high-pressure liquid chromatography/mass spectrometry to facilitate detection of trace impurities in formulated drug products. *Rapid Commun Mass Spectrom*. 2007;21(7):1255-1263.
39. Goshawk J, Eatough D, Wood M. Componentization following 3D-peak detection in the unifi scientific information system. White paper *720005480en*, Waters Corporation. 2015.
40. Lapthorn C, McCullagh M, Stead S, et al. The importance of charge isomers in quantitation; ion mobility mass spectrometry of fluoroquinolone antibiotics. *Proceedings of the 63rd ASMS Conference on Mass Spectrometry and Allied Topics*, St Louis, Missouri; May 31–June 4, 2015.
41. Souza GH, Campuzano I, Lalli PM, et al. Investigating analine isomer separation utilizing traveling wave ion mobility and polarizable drift gases. Appl. Note, *Library number 720003505en*. Waters Corporation. 2012.
42. Jurneczko E, Kalapothakis J, Campuzano I, Morris M, Barran PE. Effects of drift gas on collision cross sections of a protein standard in linear drift tube and traveling wave ion mobility mass spectrometry. *Anal Chem*. 2012;84(20):8524-8531.
43. Fasciotti M, Sanvido GB, Santos VG, et al. Separation of isomeric disaccharides by traveling wave ion mobility mass spectrometry using CO_2 as drift gas. *J Mass Spectrom*. 2012;47(12):1643-1647.
44. Bush MF, Campuzano I, Robinson CV, et al. Structural characterization of drug-like compounds by ion mobility mass spectrometry: Comparison of theoretical and experimentally derived nitrogen collision cross sections. *Anal Chem*. 2012;84:1026-1033.
45. Boschmans J, Jacobs S, Williams JP, et al. Combining density functional theory (DFT) and collision cross-section (CCS) calculations to analyze the gas-phase behaviour of small molecules and their protonation site isomers. *Analyst*. 2016;141:4044-4054.
46. Giles K, Wildgoose J, Pringle S, et al. Design and utility of a multi-pass cyclic ion mobility separator. *Proceedings of the 62nd ASMS Conference on Mass Spectrometry and Allied Topics*, Baltimore, Maryland. June 15–19, 2014.
47. Warnke S, Seo J, Boschmans J, et al. Protomers of benzocaine: Solvent and permittivity dependence. *J Am Chem Soc*. 2015;137(12):4236-4242.
48. Bull JN, Coughlan NJA, Bieske EJ. Protomer-specific photochemistry investigated using ion mobility. Mass spectrometry. *J Phys Chem A*. 2017;121:6021-6027.

SUPPORTING INFORMATION

Additional supporting information may be found online in the Supporting Information section at the end of the article.

How to cite this article: McCullagh M, Giles K, Richardson K, Stead S, Palmer M. Investigations into the performance of travelling wave enabled conventional and cyclic ion mobility systems to characterise protomers of fluoroquinolone antibiotic residues. *Rapid Commun Mass Spectrom*. 2019;1–11. https://doi.org/10.1002/rcm.8371